# Research Article

Vol. 28 (No. 4), pp. 279-291, 2025 doi: 10.5541/ijot.1681635 Published online: December 1, 2025

# Numerical Study on Channel-Driven U-Shaped Cavity Flow with Adiabatic Baffles: PEC For W/EG Mixture-Based TiO<sub>2</sub>-SiO<sub>2</sub> Hybrid Nanofluid

<sup>1</sup>\*M. Jourabian

<sup>1</sup> Department of Mechanical Engineering, Faculty of Engineering, Tarsus University, Tarsus, Mersin, Turkey E-mail: \*mjourabian@tarsus.edu.tr

Received 22 April 2025, Revised 21 August 2025, Accepted 11 November 2025

#### Abstract

Turbulent forced convection over asymmetrical cavity flows is encountered in numerous industrial applications. The importance of heat exchange or minimizing the encapsulating phenomenon has inspired thermal engineers to rely on altering the geometry of the heat transfer component (passive technique). Besides, the heat transfer capability of water and ethylene glycol (EG) solution is limited, and it depends on the working temperature and composition of the mixture. Hence, in this study, the influences of adiabatic baffles and  $\text{TiO}_2\text{-SiO}_2$  hybrid nanoparticles (NPs) on the thermal performance of binary fluid in a 2D channel-driven U-shaped cavity flow are examined using the single-phase k- $\omega$  SST model. The results indicate that for the pure aqueous solution of EG, using elongated baffles increases the average Nu number (ANN) by 87% and 67%, respectively, compared to the plain cavity flow at Re=5000 and 30000. For the cavity flow without baffles at  $U_0$ =0.6 m/s, the value of ANN decreases by 14% using  $\text{TiO}_2$ -SiO<sub>2</sub> (mixing ratio 50:50%) hybrid nanofluid (HyNf) with  $\phi$ =0.01 compared to the pure mixture flow. Inserting smaller baffles in the U-shaped cavity flow is always advantageous at all velocities of the incoming flow. It confirms that dispersing  $\text{TiO}_2$ -SiO<sub>2</sub> NPs does not enhance the heat transfer capability of the binary mixture, especially at higher Re numbers. Moreover, the simultaneous substitution of the pure mixture in the plain cavity flow with the  $\text{TiO}_2$ -SiO<sub>2</sub> HyNf in the cavity flow equipped with baffles cannot be recommended.

**Keywords:** Cavity flow; turbulent forced convection; PEC; nanofluid; baffle; water/EG mixture.

#### 1. Introduction

#### 1.1 Classification of Cavity Flows

Forced convection heat transfer over cavity flows is encountered in numerous industries and engineering applications, including wind barriers in solar collectors, thermal design of electronic components, thermal regenerators, ribbed heat exchangers, lubrication technology, microelectronic chips, autoclaves, nuclear reactors, and the clearance gap of a grooved turbine blade tip (turbine blade cooling).

Results of the smoke flow visualization for the laminar separating flow, given by Sinha et al. [1], revealed that there are four types of flow patterns within cavities, including

- 1. Shallow closed cavity flow (when the ratio between the depth and width of the cavity is lower than 0.1),
- 2. Shallow open cavity flow (the ratio is between 0.1 and 0.5)
- 3. Open cavity flows (the ratio is between 0.5 and 1.5), and
  - 4. Deep cavity (the above ratio is higher than 1.5).

Nevertheless, as Zdanski et al. [2] confirmed, the experimental data presented by Sinha et al. [1] were not adequate for recognizing the multifarious features of cavity flows, particularly the common sorting of a cavity flow as open or closed. According to Zdanski et al. [2], the vortex encapsulation phenomenon (thermal insulating mechanism) is installed when the aspect ratio (AR) of the cavity flow is

lower than 10.0, or the oncoming turbulence level is below 7%, or the Re number based on the depth of the cavity is lower than 12000. When the eddy encapsulation occurred, the convective action due to the external flow was isolated from the bottom surface of the cavity (the heat loss by convection was significantly abated). As Zdanski et al. [2] found, the rupture of the capsule took place for 10 < AR < 12. In this case, the oncoming flow attached along the cavity floor, and convective effects became highly effective.

Mesalhy et al. [3] numerically investigated the steady, incompressible, and turbulent flow over the shallow cavity. They indicated that the cavity behaved as a shallow open cavity when the AR of the cavity was small, around 4.0 or 5.6. The flow was characterized by a single elongated eddy. There were two smaller eddies inside the bigger eddy, one close to the upstream side wall and the other close to the downstream side wall. As the cavity AR increased, the cavity flow behaved as a shallow closed cavity. It was noticed for AR>7.0. The flow was characterized by an eddy behind the upstream side wall. Another eddy was created in front of the downstream side wall. They emphasized that the flow over a shallow closed cavity had the chance to impinge on the bottom wall of the cavity. The location at which the flow impinged on the bottom wall changed with the cavity AR and the mean air velocity in the channel.

# 1.2 Effects of Baffle and NF on Cavity Flow

\*Corresponding Author Vol. 28 (No. 4) / 279

The importance of heat exchange in numerous engineering applications has motivated researchers to find ways for enhancing forced convection heat transfer. Among the practices are the passive techniques such as imposing geometric changes [4], inserting adiabatic baffles at the top wall [5-6], and/or adjusting the heater's position [7-9].

Ma et al. [5] numerically studied the forced convection heat transfer of multi-walled carbon nanotubes (MWCNT)-Fe<sub>3</sub>O<sub>4</sub>/water HyNf over the forward-facing step (FFS) and backward-facing step (BFS) channels with a baffle on the top wall. It was illustrated that the baffle at the top wall noticeably affected the flow pattern and heat transfer characteristics. As the baffle elongated, the size of the recirculation zone downstream of the BFS decreased. To enhance the heat transfer rate, the length of the baffle increased, and the baffle moved towards the BFS.

Navaneethakrishnan and Muthtamilselvan [6] scrutinized the effects of magnetohydrodynamic (MHD) mixed convection on the flow structure and heat transfer characteristics within a vented channel-driven cavity. They considered a corner heater and an adiabatic rod positioned vertically downward from the top wall of the channel. The variations of the Re number significantly affected the fluid flow and heat distribution. Increasing the length of the rod enhanced the value of ANN (an improved heat transfer). However, altering the thickness of the rod did not significantly enhance it.

Note that the effectiveness of passive techniques (geometric changes and baffles) is limited in other applications. So, the best solution may be nanofluids (NFs), the colloidal solutions created by metals, metal oxides, CNT, or silica carbide NPs having a higher thermal conductivity added to a base fluid such as water, EG, or oils. The acquired NF has a thermal conductivity higher than that of the base fluid

Nouraei et al. [7] numerically investigated the laminar flow (mixed convection) of water/Cu NF in an open cavity of semicircular shape with various positions of hot surfaces at the angle of 45°. At *Re*=100.0 (dominance of the fluid momentum in comparison with the viscous force), the effect of the volume fraction of NPs was reduced. The best heat transfer performance was achieved using a higher volume fraction of NPs, and the heat transfer was boosted by 8-19% due to the addition of NPs to pure water.

Mixed convection heat transfer of the unsteady NF flow in an open cavity heated from below with uniform temperature was numerically scrutinized by Mehrez et al. [10]. Dispersing Cu, CuO, Al<sub>2</sub>O<sub>3</sub>, or TiO<sub>2</sub> NPs in the pure water altered the behavior of the flow. It diminished the flow intensity and enlarged the thickness of the thermal boundary layer (TBL). The sensitivity of the heat transfer to the type of NPs was accentuated. The highest values were gained with copper NPs, the lowest ones with TiO<sub>2</sub> NPs, and intermediate values with CuO NPs. Mehrez et al. [10] proved that these different perceived behaviors were qualified by the difference between the thermophysical properties of various NPs.

# 1.3 Pure Aqueous Solutions of EG

EG, when correctly inhibited for corrosion control, can be utilized as antifreeze and heat transfer fluid. Although water is a much better engine coolant, the trouble with water is that it freezes or boils at extreme temperatures. EG effectively reduces the freezing point of water, giving low volatility while possessing comparatively low corrosivity when appropriately inhibited. EG is colorless, essentially odorless liquid. It is miscible with water and numerous organic mixtures.

The chief application of EG is as a medium for convective heat transfer (CHT), for instance, in direct absorption solar collectors (DASC), car radiators, liquidcooled computers, and air conditioning devices. The optimum concentration of glycol is related to the form of protection needed by the application. If the fluid should avoid equipment damage during idle hours in cold temperatures, such as winterizing coils in an HVAC system, the volume of EG could be 30%, and it could form a slush and flow in any space. Keep in mind that the user should avoid excessive glycol concentration because it raises the initial price and it unfavorably affects the thermophysical properties. Physical properties (such as density, specific heat, thermal conductivity, and viscosity) for aqueous solutions of EG are listed by ASHRAE [11]. Densities for aqueous solutions of industrially inhibited glycols are higher than those for pure glycol and water alone. Compared to the pure EG and water, the densities for the water/EG mixture are greater.

Xu et al. [12] found that the EG/water mixture (as the base liquid) gives the reduced graphene oxide (RGO)/water-EG NF an anti-freeze property in cold weather. They found that the RGO/water-EG NF exhibited higher thermal conductivity compared to the RGO/water NF.

Peyghambarzadeh et al. [13] emphasized that the EG withstood much greater temperature extremes. Based on Peyghambarzadeh et al. [13], the EG/water mixture gave acceptable cooling capabilities of water while withstanding extreme temperatures. Yiamsawas et al. [14] stated that compared to water, the aqueous solutions of EG were more helpful since the viscosity of the EG/W mixture was less than that of EG, and therefore, the necessary pumping power diminished.

#### 1.4 Water/EG Mixture-based NFs

Generally speaking, water and EG possess poor convective heat transfer performance, and hence, to attain the essential heat transfer, high compactness and efficacy of thermal systems are mandatory. A great number of numerical works are devoted to understanding the effects of dispersing single/hybrid NPs in an EG/W mixture, as a binary heat transfer fluid. The latter one can be created by suspending hybrid metallic/metallic oxide NPs (with a size smaller than 100 nm) in the binary fluid. The thermal conductivity and dynamic viscosity of water/EG mixture-based NFs were estimated by the well-known classical models, or they were extracted from the relevant lab-scale experimental measurements.

Yiamsawas et al. [14] experimentally determined the viscosity of TiO<sub>2</sub> and Al<sub>2</sub>O<sub>3</sub> NPs suspended in a mixture of EG/water (20:80%). They highlighted that the main cause of the disparity between experimental data and theoretical models is that the models were developed based on low concentrations of NPs. In addition, the NP size (or configurations of NPs) was not incorporated in the classical models, which affected the accuracy of theoretical predictions.

Kumaresan and Velraj [15] measured the thermophysical properties of water/EG mixture-based carbon nanotube (CNT) NFs. They illustrated that the measured data showed a noticeable deviation from the predicted values given by the Pak and Cho correlation, and the level of the under-

prediction enlarged with an augmentation in multi-walled carbon nanotubes (MWCNT) concentration. It was due to the spontaneous filling of nanotubes with water in a restricted way, which augmented the NF mass for a given volume. It was indicated that this discrepancy greatly affected the evaluation of the flow and heat transfer features. The specific heat equation (the equilibrium-based equation extensively used in experimental and numerical convective heat transfer studies) provided considerably lower values compared to the measured data. The deviation was probably due to the existence and promotion of definite thermal transport mechanisms. In other words, the theoretical correlation did explain the size and surface effects in CNTs.

For the effective thermal conductivity of NFs, the experimental data were much higher than the predicted values given by the well-known correlations. The classical models failed to consider the effects of particle size, nanolayering, clustering between NPs and base fluid, Brownian motion, and complex kinetics of MWCNT aggregation at higher temperatures (T=40°C).

Finally, the relative viscosity ratio of water/EG mixture-based CNT NFs generally was enhanced by augmenting the concentration of NPs. At lower volumetric concentrations ( $\phi$ =0.15%), this ratio did not change significantly with the temperature. Nevertheless, for higher concentrations ( $\phi$ =0.3%, 0.45%), this ratio was significantly affected by the temperature.

At lower temperatures, the viscosity ratio for all NFs was low (between 1.0 and 2.0), making them a proper choice for cooling applications (the lowest penalty in the pumping power). Nonetheless, at higher temperatures ( $T \ge 20^{\circ}$ C), the viscosity ratio was higher than 3.0. It reduced the helpful thermal transport effects of such NFs. The Einstein model underpredicted the viscosity ratio even at a concentration of  $\phi$ =0.15% (It did not illustrate the temperature-dependent variation of the viscosity ratio). The Einstein model did not account for the effects of the shape and size of CNTs.

By using the transient-hot wire method, Sundar et al. [16] measured the thermal conductivity of a water/EG mixture-based Fe<sub>3</sub>O<sub>4</sub> NF. They observed that the Hamilton-Crosser model did not predict the temperature-dependent variations of the thermal conductivity. They noticed that existing thermal conductivity models (theoretical) for NFs did not agree with the measured data.

Bhanvase et al. [17] experimentally predicted the convective heat transfer performance of  $TiO_2$  NFs (Pr=14.86) based on a water/EG (60:40%) mixture in a long copper pipe at Re=1200. The effective thermal conductivity and viscosity of NF suspensions were predicted theoretically by the Maxwell and Einstein models, respectively. With the addition of  $TiO_2$  NPs (0.5 vol.%), the heat transfer coefficient was considerably enhanced (105%). Compared to the deionized water, there was a 60% augmentation in the heat transfer coefficient using  $TiO_2$  NPs with  $\phi$ =0.1%.

Nabil et al. [18] experimentally measured the properties of TiO<sub>2</sub>-SiO<sub>2</sub> HyNf ( $0.5 \le \phi \le 3.0\%$  with a volume ratio of 50:50%) in a mixture of water and EG (volume ratio of 60:40%). They concluded that the water/EG mixture-based TiO<sub>2</sub>-SiO<sub>2</sub> HyNf behaved as a beneficial heat transfer fluid for concentrations  $\phi \ge 1.5\%$ .

The thermal conductivity and dynamic viscosity of boron nitride (BN) NFs, synthesized using a water/EG mixture (60:40%) were measured by Michael et al. [19]. When the experimental data were compared against the well-established classical models, they observed that theoretical

models underestimate the thermophysical properties of NFs because they do not consider several imperative aspects, for instance, the size of NPs, Brownian motion, and NP aggregation.

Hamid et al. [20] measured the thermo-physical properties of  $TiO_2$ -SiO<sub>2</sub> NPs (with  $\phi$ =1.0%) suspended in a base fluid (mixture of water and EG with a 60:40% volume ratio). Five mixture ratios of  $TiO_2$ -SiO<sub>2</sub> NPs (20:80, 40:60, 50:50, 60:40, and 80:20) were examined. Using the properties enhancement ratio (PER), they proved that the ratio of 50:50 was not a good choice to enhance the heat transfer compared to other ratios. The best mixture ratios reported were 40:60 and 80:20, in which the combined effects due to enhanced thermal conductivity and dynamic viscosity were more advantageous.

Sen et al. [21] numerically investigated the MHD flow of a water/EG mixture-based CoFe<sub>2</sub>O<sub>4</sub>-TiO<sub>2</sub> HyNf over a stretchable cylinder with a non-linear radiation and heat source. They determined that the efficiency of heat transfer was higher for HyNf than for single NF and base binary fluid.

# 2. Motivation and Objective

Generally speaking, most works on cavity flows were accomplished for rectangular and symmetrical (the upstream wall height equal to the downstream one) cavities. The shape of cavity flows varies greatly in electronic cooling systems, and they are still unexplored. While there are some articles published on non-rectangular cavities [4, 7], there is a necessity to analyze the turbulent forced convection heat transfer over asymmetrical cavity flows. To the best of my knowledge, the channel-driven U-shaped cavity flow (consisting of a downward-facing cavity and an upward-facing cavity) equipped with baffles attached to the top wall has never been researched.

As Azmi et al. [22] emphasized, there are limited works that use the water/EG mixture NFs in the estimation of the forced convection heat transfer. The use of TiO2 NPs as conducting solids in the formulation of HyNf was reported due to its benefits, for example, ease of accessibility, handling safety, greater heat transfer coefficients, and exceptional chemical and physical stability without any further stabilizer. On the other hand, Shi et al. [23] numerically investigated the pressure drop, particle distribution, and heat transfer of SiO<sub>2</sub>/water NFs flowing through a turbulent tube. They found that  $\Delta P$  was enhanced considerably after adding SiO<sub>2</sub> NPs and amplified with augmenting the Re number. The boosted viscosity hindered the motion of NF, and it induced more irregular migration of NPs. Once the inlet velocity was small, the intensification in  $\Delta P$  caused by SiO<sub>2</sub> NPs was comparatively high. As Nabil et al. [18] underlined, further experimental/numerical heat transfer studies are essential to approve the suitability of water/EG mixture-based TiO2-SiO2 HyNf.

The single-phase turbulent forced convection heat transfer for the water/EG (with a volume ratio of 60-40%) mixture-based TiO<sub>2</sub>-SiO<sub>2</sub> (50-50%) HyNf over a 2D channel-driven U-shaped cavity flow is explored numerically in this paper. The cavity is heated at a constant temperature (*T*=343K). Instead of theoretically predicting the properties of mixture-based HyNf, the temperature-dependent properties are obtained from the available experimental data [18, 20].

The Reynolds-Averaged Navier-Stokes (RANS) and energy equations are solved using the k- $\omega$  SST model in OpenFOAM. Finally, I would answer these questions:

- (1) Is the presence of  $TiO_2$  NPs in the binary mixture able to reduce the negative effects due to  $SiO_2$  NPs?
- (2) How does the variation of the NP volume fraction and mixing ratio of hybrid NPs affect the heat transfer capability of the water/EG mixture?
- (3) Does the introduction of baffles increase the performance evaluation criterion (PEC) for the aqueous solution of EG? Note that baffles installed on the top wall may create extra recirculating eddies (as an insulating impact on the heat transfer).

#### 3. Numerical Method

#### 3.1 Computational Domain

In Figure 1, the geometry considered in this investigation is illustrated. It is a 2D horizontal channel with a U-shaped cavity heated at constant temperature (T=343K). The water/EG mixture-based TiO<sub>2</sub>-SiO<sub>2</sub> HyNf is introduced to the duct at a constant velocity ( $U_0$ =0.1, 0.3, 0.6 m/s) and temperature ( $T_0$ =293K). The top wall and the upstream and downstream walls are adiabatic. The height of the inflow and outflow sections (H) is equal to h=0.042m.

Two more developed models are studied, one with an adiabatic baffle with a length of h=0.042m, and the other one with an elongated baffle (2×h). In this study, the positions of adiabatic baffles within the cavity flow are fixed as well as their thickness. All the walls of the computational domain are treated as no-slip boundary conditions (BCs).

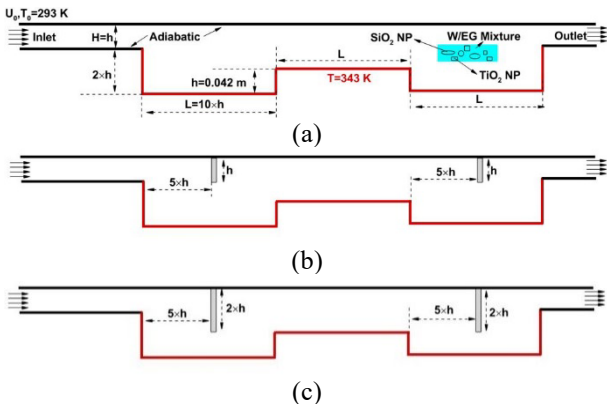


Figure 1. Schematic diagrams of channel-driven U-shaped cavity flows without baffle (a), with baffle (b), and elongated baffle (c).

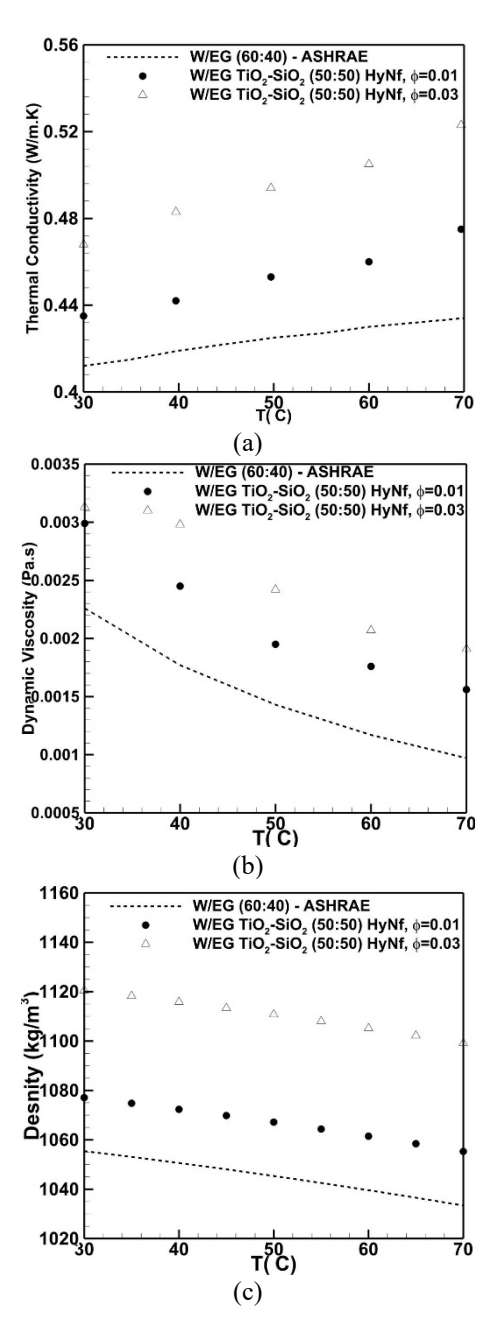
The incoming water/EG (with a volume ratio of 60-40%) mixture flow (with  $Pr_b$ =19.20 at T=303K) is 2D, steady-state, turbulent, fully developed, and incompressible. Considering the analysis of heat transfer in high Re number flows, the forced convection is assumed to be prevailing, and hence, the natural convection is disregarded. The working fluids are assumed to be single-phase and Newtonian fluids. The thermophysical properties of pure binary fluid and HyNf are defined as a function of temperature and NP volume fraction.

# 3.2 Thermophysical Properties of HyNf

In the present study, to get a clear understanding of the effects of hybrid NPs on the thermal performance of the binary mixture, the lab-scale experimental data of thermal conductivity and dynamic viscosity given by [18, 20] are implemented.

In Figure 2, the thermophysical properties for aqueous solutions of EG dispersed with TiO<sub>2</sub>-SiO<sub>2</sub> hybrid NPs are given. Nabil et al. [18] measured the thermal conductivity

and dynamic viscosity of TiO2-SiO2 HyNf in a water/EG mixture (for concentrations  $0.5 \le \phi \le 3.0\%$  and temperatures 30≤T≤80°C) using KD2 Pro Thermal Properties Analyser and Brookfield LVDV III Ultra Rheometer, respectively. The average diameters for TiO<sub>2</sub> and SiO<sub>2</sub> NPs were equal to 30-50nm and 22nm, respectively. The densities for TiO<sub>2</sub> and SiO<sub>2</sub> NPs were equal to 4230 and 2220 kg/m3, respectively. They studied HyNf in a base fluid mixture of distilled water and EG with a volume ratio of 60:40%. The HyNf was prepared by mixing both single NFs by a 50:50% (TiO2:SiO2) volume ratio. The TiO2-SiO2 HyNf were subjected to the process of mixing by using a magnetic stirrer and sonification. They validated the thermal conductivity and dynamic viscosity measurements of water/EG (60:40) mixture against ASHRAE [11]. Regarding the thermal conductivity of the aqueous solution of EG, the maximum deviation was found to be 1.6% (the measurement was reliable). The viscosity data were also in good agreement with the data from ASHRAE [11]. It showed that the dynamic viscosity declined with the increase of temperature.



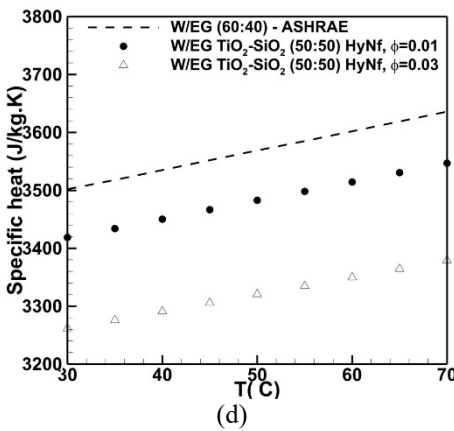


Figure 2. Thermal conductivity (a), dynamic viscosity (b), density (c), and specific heat (d) for aqueous solutions of EG with/without TiO<sub>2</sub>-SiO<sub>2</sub> hybrid NPs.

The thermal conductivity of water/EG mixture-based TiO2-SiO2 HyNf improved with increasing concentration and temperature. Compared to the pure mixture, the maximum enhancement (22.8%) was found at a concentration of  $\phi$ =3.0% and a temperature of T=80°C. The collision of hybrid NPs occurred at a higher rate at higher temperatures, thus transporting more kinetic energy and resulting in improved thermal conductivity. The higher concentration of HyNf and the greater number of NPs dispersed in the base mixture resulted in the augmentation of the surface-to-volume ratio and collisions between NPs. This effect was also due to the Brownian motion of NPs in the base fluid. The dynamic viscosity of HyNF was higher than the base mixture, and it amplified with the NP concentration. It was due to the augmentation in the fluid internal shear stress when hybrid NPs were added to the base mixture.

At higher concentrations ( $\phi$ =3.0%), the enhancement in dynamic viscosity concerning NP concentration was much higher than the base mixture. The interaction between hybrid NPs and base fluid (water/EG) also contributed to the greater augmentation compared to single NF. The viscosity of HyNF followed the base mixture trend, which diminished with the increment of the temperature. The intermolecular interactions between molecules became weaker when the temperature rises, and therefore, reducing the dynamic viscosity. The viscosity ratio was enhanced with the rising NP concentration. Nevertheless, it was slightly changed with temperature (small fluctuations).

The lowest average value of the relative viscosity (with a percentage increase of 25.9%) was obtained for  $\phi$ =0.5%. Besides, the highest average value of the relative viscosity (with a 62.5% increment) was achieved for  $\phi$ =3.0%. The maximum value of the relative viscosity was observed for  $\phi$ =3.0% at a temperature of T=80°C. In general, the relative viscosity within the present range of  $\phi$  and temperature increased from 21.3% to 80.0% compared to the mixture. The fluctuation of the relative viscosity in the temperature range (30°C $\leq$ T<80°C) was not well understood. Nonetheless, this outcome was due to the difference in structure and thickness of the diffused fluid layers around NPs in the base mixture, which influenced the effective concentration and viscosity of the suspension.

The effective density and heat capacity of water/EG mixture-based TiO<sub>2</sub>-SiO<sub>2</sub> HyNf at a reference temperature were acquired via the following expressions:

$$\rho_{hnf} = (1.0 - \phi)\rho_{hf} + \phi\rho_{hnp} \tag{1}$$

$$\left(\rho c_p\right)_{hnf} = (1.0 - \phi)\left(\rho c_p\right)_{hf} + \phi\left(\rho c_p\right)_{hnn} \tag{2}$$

#### 3.3 Governing Equations

The single-phase turbulent forced convection heat transfer of HyNf is solved by the Reynolds-Averaged Navier-Stokes (RANS) equations. The time-averaged velocity, pressure, and temperature fields are resolved. The Reynolds stresses are estimated by the eddy viscosity models. These models apply the turbulent viscosity for relating the turbulent stresses and heat fluxes to the mean strain rate. Furthermore, the radiation heat transfer and heat generation are assumed to be insignificant.

Regarding the above assumptions, the time-averaged mass, momentum, and energy conservation equations can be written as [24-27],

$$\frac{\partial \bar{u}}{\partial x} + \frac{\partial \bar{v}}{\partial y} = 0 \tag{3}$$

$$\rho_{hnf}\left(\overline{u}\,\frac{\partial\overline{u}}{\partial x}+\overline{v}\,\frac{\partial\overline{u}}{\partial y}\right)=-\frac{\partial\overline{p}}{\partial x}+\left[\left(\mu_{hnf}+\mu_{t}\right)\left(\frac{\partial^{2}\overline{u}}{\partial x^{2}}+\frac{\partial^{2}\overline{u}}{\partial y^{2}}\right)\right]\ (4)$$

$$\rho_{hnf}\left(\bar{u}\frac{\partial\bar{v}}{\partial x} + \bar{v}\frac{\partial\bar{v}}{\partial y}\right) = -\frac{\partial\bar{v}}{\partial y} + \left[\left(\mu_{hnf} + \mu_{t}\right)\left(\frac{\partial^{2}\bar{v}}{\partial x^{2}} + \frac{\partial^{2}\bar{v}}{\partial y^{2}}\right)\right] \tag{5}$$

$$\begin{split} \rho_{hnf} \left( c_p \right)_{hnf} \left( \overline{u} \, \frac{\partial \overline{T}}{\partial x} + \overline{v} \, \frac{\partial \overline{T}}{\partial y} \right) &= \left( k_{hnf} \, + \right. \\ \left. \frac{\left( c_p \right)_{hnf} \times \mu_t}{Pr_t} \right) \left( \frac{\partial^2 \overline{T}}{\partial x^2} + \frac{\partial^2 \overline{T}}{\partial y^2} \right) \end{split} \tag{6}$$

#### 3.4 Turbulence Modeling

The standard SST  $k-\omega$  model [28-29] utilizes the effectiveness of Wilcox  $k-\omega$  and  $k-\epsilon$  models at favorable regimes (near solid walls and in the freestream).

As Araujo and Rezende [30] emphasized, the SST k- $\omega$  model (as a RANS turbulence model) is recommended for cases with adverse pressure gradient and flow separation. This model presents a better treatment in the near-wall regions compared to other RANS models.

Sekrani et al. [31] clarified that the SST k-ω model gave the most precise estimates for both the Nu number and the friction factor.

Jehad et al. [32] analyzed the turbulent flow over the BFS with three turbulence models called the standard k- $\epsilon$ , realizable k- $\epsilon$  and SST k- $\omega$ . They found that the SST k- $\omega$  model exhibited a satisfactory agreement against experimental data given by [33] in terms of the size of the reattachment zone.

Nevertheless, interestingly, the SST k- $\omega$  model performs poorly in calculating the turbulence intensity and shear stress in the recirculation region (underestimating the eddy viscosity compared to experimental data).

In OpenFOAM package [34], the production limiter is added in the standard SST k- $\omega$  model. In OpenFOAM, the transport equations for the turbulent kinetic energy (TKE) and specific dissipation rate are given as [35-36]:

$$\frac{\partial}{\partial x_i}(\rho k u_i) = \frac{\partial}{\partial x_i} \left[ (\mu + \sigma_k \mu_t) \frac{\partial k}{\partial x_i} \right] + P_k - \beta^* \rho k \omega \tag{7}$$

$$\frac{\partial}{\partial x_{i}}(\rho\omega u_{i}) = \frac{\partial}{\partial x_{i}}\left[(\mu + \sigma_{\omega}\mu_{t}).\frac{\partial\omega}{\partial x_{i}}\right] + \frac{\gamma\rho}{\mu_{t}}P_{k} - \beta\rho\omega^{2} + 2(1 - F_{1})\frac{\rho\sigma_{\omega 2}}{\omega}\frac{\partial k}{\partial x_{i}}\frac{\partial\omega}{\partial x_{i}} \tag{8}$$

$$P_{k} = \tau_{ij} \frac{\partial u_{i}}{\partial x_{i}} = \left[ \mu_{t} \left( 2S_{ij} - \frac{2}{3} \frac{\partial u_{k}}{\partial x_{k}} \delta_{ij} \right) - \frac{2}{3} \rho k \delta_{ij} \right] \frac{\partial u_{i}}{\partial x_{i}}$$
(9)

$$F_1 = \tan h(\Phi_1^4), \qquad F_2 = \tan h(\Phi_2^2)$$
 (10)

$$\Phi_{1} = min \left[ max \left( \frac{\sqrt{k}}{\beta^{*} \omega y}, \frac{500 \mu}{\rho y^{2} \omega} \right), \frac{4\rho \sigma_{\omega 2} k}{CD_{k\omega} y^{2}} \right]$$
 (11)

$$CD_{k\omega} = max \left( 2\rho \frac{\sigma_{\omega 2}}{\omega} \frac{\partial k}{\partial x_i} \frac{\partial \omega}{\partial x_i}, 10^{-10} \right)$$
 (12)

$$\Phi_2 = max\left(\frac{2\sqrt{k}}{\beta^*\omega y}, \frac{500\nu}{y^2\omega}\right) \tag{13}$$

$$\mu_t = \frac{\rho a_1 k}{\max(a_1 \omega, F_2 S)}, \quad S = \sqrt{S_{ij} S_{ij}}, \quad S_{ij} = \frac{1}{2} \left( \frac{\partial u_i}{\partial x_j} + \frac{\partial u_j}{\partial x_i} \right) \quad (14)$$

The empirical constant  $\chi$  is evaluated based on,

$$\chi = \chi_1 F_1 + \chi_2 (1 - F_1) \tag{15}$$

Keep in mind that  $\chi_1$  and  $\chi_2$  are extracted from k-ω and k-ε models, respectively. Also, all is a constant and estimated experimentally (0.31),  $F_2$  is the blending (damping) function. The values of constants for the SST k-ω model were provided by Torabi et al. [24].

#### 4. Flow and Heat Transfer Characteristics

In this study, the inlet channel height-based Re number is defined as,

$$Re = \frac{\rho_{hnf} \times U_0 \times H}{\mu_{hnf}} \tag{16}$$

The surface Nu number on the heated surfaces and ANN along the cavity walls are calculated to present the convective performance of coolant,

$$Nu = \frac{h_{hnf} \times H}{k_{hf}} \tag{17}$$

$$ANN_{cavity\ flow} = ANN_{BFS1} + ANN_{BFS2} + ANN_{FFS1} + \\ ANN_{FFS2} + ANN_{lowerwall1} + ANN_{lowerwall2} + \\ ANN_{lowerwall3}$$
 (18)

For the single-phase turbulent forced convection flow, the friction factor is estimated by,

$$f = \frac{2\Delta P}{\rho_{hnf} \times U_0^2} \times \frac{H}{(3 \times L)} \tag{19}$$

The FOM is characterized as the ratio between Mouromtseff (*Mo*) numbers of HyNF and pure mixture as,

$$FOM = \frac{Mo_{hnf}}{Mo_{bf}} = \frac{\rho_{hnf}^{0.8} k_{hnf}^{0.6} c_{p,hnf}^{0.4}}{\mu_{hnf}^{0.4}} \times \frac{\mu_{bf}^{0.4}}{\rho_{bf}^{0.8} k_{bf}^{0.6} c_{p,bf}^{0.4}}$$
(20)

In this study, the  $PEC_{baffle}$  and  $PEC_{hnf}$  characterizes the influences of adiabatic baffles and concentration of HyNf, respectively.

Keep in mind that *PEC*<sub>tot</sub> designates the ratio of the Nu number of HyNf in U-shaped cavity flow equipped with baffles to that of the pure mixture (binary fluid) in the U-shaped cavity flow without baffles divided by the ratio of the

friction factor of HyNf in the cavity flow with baffles to that of the pure mixture in the cavity flow without baffles,

$$PEC_{baffle} = \frac{\frac{Nu_{baffle}}{Nu_{no \ baffle}}\Big|_{\phi = const}}{\left[\frac{f_{baffle}}{f_{no \ baffle}}\right]_{\phi = const}^{\frac{1}{3}}}\Big|_{\phi = const}$$
(21)

$$PEC_{hnf} = \frac{\frac{Nu_{hnf}}{Nu_{bf}}\Big|_{baffle,no\ baffle}}{\left[\frac{f_{hnf}}{f_{bf}}\right]^{\frac{1}{3}}}\Big|_{baffle,no\ baffle}$$
(22)

$$PEC_{tot} = \frac{\frac{Nu_{hnf,baffle}}{Nu_{bf,no\ baffle}}}{\left[\frac{f_{hnf,baffle}}{f_{bf,no\ baffle}}\right]^{\frac{1}{3}}}$$
(23)

It must be emphasized that when  $PEC_{np}>1.0$ , the HyNf is preferred compared to the pure base mixture in U-shaped cavity flows with/without adiabatic baffles.

# 5. Numerical Result and Discussion5.1 Grid Independence and Solution

All 2D numerical simulations have been performed on a desktop PC with a CPU Intel(R) Core i5, 2.9 GHz, and 24.00 GB of RAM. The aforementioned governing equations and the turbulence model are solved via the open-source code OpenFOAM. It is a free-source CFD package providing C++ codes. The existing computational modules permit the user to accomplish the desired objectives effectively. The library blockMeshDict is used to create the mesh, and the solver buoyantSimpleFoam is applied in simulations.

In the object file fvSolution, the values for the residualControl and relaxationFactors are equal to  $10^{-7}$  and 0.4, respectively. Additionally, in the object file fvSchemes, divSchemes is selected as bounded Gauss upwind. At the walls including the downward-facing cavity and an upward-facing cavity, wall functions are used for each turbulence variable. For the TKE, kqRWallFunction is applied. It is a zero-gradient BC. For the specific dissipation rate, omegaWallFunction is used.

For the pure aqueous solution of EG in the cavity flow without baffles at Re=5000, three mesh sizes (excluding the inlet and outlet regions) with the mesh refinement close to cavity walls are selected: 23360, 52560, and 118260. For the mesh size equal to 52560, the SIMPLE solution converges in 55696 iterations, and the execution time is approximately 37.06 hours. After performing command foamLog, the final values for  $U_x$  and  $U_y$  are  $6.91\times10^{-9}$  and  $9.75\times10^{-8}$ , respectively. Besides, the maximum value of  $y^+$  for the three lower walls and steps (FFS or BFS) is equal to  $3.61\times10^{-2}$  and 1.73, respectively.

As the mesh size enlarges from 23360 to 52560, the total ANN increases by 1.69%. When the fine grid is applied, the value of total ANN decreases by 0.84% compared to the medium size of the mesh. Also, the values of  $Nu_{max}$  on the first and third floors of the cavity reduce by 1.3% and 7%, respectively. However, the execution time is enhanced by more than 60%. So, the medium size of the grid is selected for the computational domain in this paper. The mesh refinement study was performed after a careful examination

of the large eddy simulation (LES) findings of the turbulent flow over a BFS given by Akselvoll and Moin [37]. Mesh refinements close to solid walls were visualized in my previous work [38].

#### 5.2 Model Validation

Xie and Xi [39] investigated the geometry effect (changeable bottom wall length and step height) on fluid flow and heat transfer characteristics over a single backwardforward facing pair at Re=700 using the direct numerical simulation (DNS). The temperature of the bottom wall is constant ( $T_h$ =313K), while the walls of the horizontal channel are thermally insulated. The air flow (Pr=0.71) at the inflow opening was fully developed for U (as the streamwise velocity) with a uniform temperature ( $T_0$ =283K). The number of computational cells in the cavity flow is equal to 36000. To validate the time-mean surface Nu number (SNN) along the bottom wall inside the cavity, the following case is selected: the inlet channel height is equal to the step height h=0.015m, and the bottom wall length is fixed as 14×h. An acceptable agreement between the present results and the ones given by [39] is obtained in Figure 3.

Abdellahoum et al. [40] and Abdellahoum and Mataoui [41] numerically evaluated the turbulent forced convection of various NFs (consisting of Cu, CuO, Ag, and Al<sub>2</sub>O<sub>3</sub> NPs with  $0.0 \le \phi \le 0.2$  in water) over a heated shallow cavity in a horizontal channel at  $4 \times 10^4 \le Re \le 10^5$ .

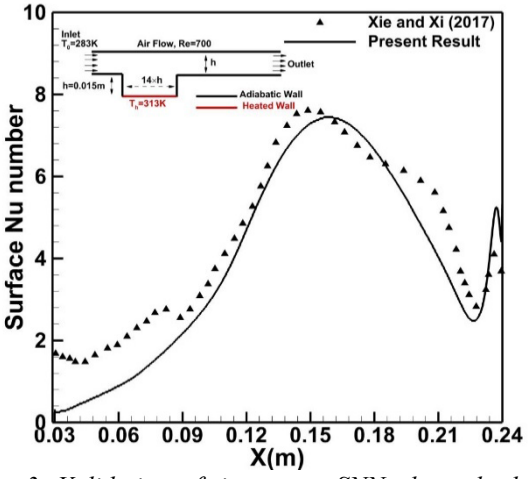


Figure 3. Validation of time-mean SNN along the bottom wall of cavity for the air flow against Xie and Xi [39].

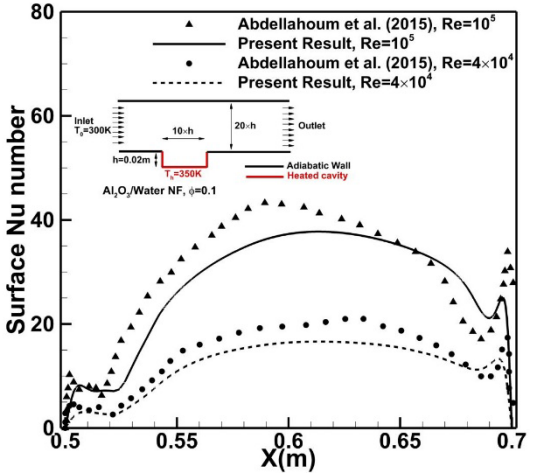


Figure 4. Validation of SNN along the bottom surface of cavity for the single NF flow against Abdellahoum et al. [40].

In Figure 4, the 2D computational domain as the second validation case is illustrated. The length of the upstream section is equal to  $25 \times h$ , and the length of the horizontal channel in the downstream section and the height of the channel (in the vertical direction) is equal to  $55 \times h$  and  $20 \times h$ , respectively. The aspect ratio  $(AR_c)$  between the width and height of the rectangular cavity is equal to 10.0, and hence, the elongated cavity is a backward/forward-facing step pair. The cavity walls are heated at a constant temperature  $T_h$ =350K while the other walls are adiabatic. At the inlet of the computational domain, fixed values are enforced as velocity components  $U=U_0$ , V=0, and ambient temperature  $(T_0=300K)$ .

For the closure of governing equations of fluid flow and heat transfer, the SST k- $\omega$  model in the single-phase framework was implemented. The thermophysical properties of all NFs were presumed to be fixed, and they are given in Table 1 for Al<sub>2</sub>O<sub>3</sub>/water NF. The dynamic viscosity and thermal conductivity of NFs (as a dilute suspension of small spherical particles in a base fluid) were calculated using the Brinkman and Maxwell-Garnett (MG) models, respectively. The effective density and heat capacity of NFs were acquired at a reference temperature using the Pak and Cho correlation and thermal equilibrium model, respectively.

Table 1. Thermophysical properties of alumina/water NF with  $\phi$ =0.1 ( $Pr_{nf}$ =5.6).

Property	Value	
Specific heat [j/kg.K]	3131.89828	
Density [kg/m³]	1294.39	
Dynamic viscosity [kg/m.s]	0.00130525	
Thermal conductivity [W/m.K]	0.80725567	

In Figure 4, the value of SNN along the cavity bottom is compared against [40-41], and a satisfactory agreement is achieved. The mesh size in the cavity flow is equal to 19200. It confirms that the increase of Re number enhances the heat transfer for  $\phi$ =0.1. Abdellahoum and Mataoui [41] also emphasized that the increment of NP volume fraction improved the heat transfer (the sum of average Nu number on heated surfaces) moderately and linearly. Unfortunately, researchers [40-41] did not examine how the theoretical values for the NF thermophysical properties may affect the accuracy of numerical results.

#### 5.3 Aqueous Solutions of EG Without Hybrid NPs

The investigation of the effects of adiabatic baffles on the fluid dynamics and heat transfer is of great importance in various engineering domains. The presence of baffles in cavity flows may modify the flow structures significantly. As revealed by Ma et al. [5], when the length of adiabatic baffles augments, the size of the recirculation region downstream of the BFS diminishes.

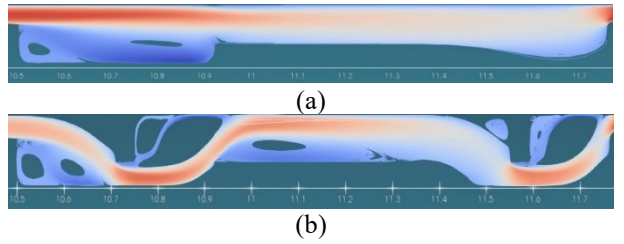


Figure 5. Streamlines for the pure mixture in the cavity flow without baffles (a), with elongated baffles (b)

In Figure 5, for the pure binary fluid flow at  $U_0$ =0.1 m/s, the streamlines in the cavity flow with/without elongated baffles are given.

In the absence of any baffles, a main clockwise recirculating eddy and a secondary counterclockwise one at the left bottom corner are created over the first floor of the cavity. The presence of baffles plays a crucial role in minimizing the encapsulating phenomenon [2]. Baffles may direct the cold fluid throughout the beneath of the U-shaped cavity (inner cavity region).

Adding baffles maximizes the interaction between the incoming fluid flow and cavity walls while reducing the sizes of both recirculating eddies. Additionally, the above arrangement of baffles generates one recirculating eddy (as a negative outcome) over the middle floor of the cavity. The turbulent flow passing over the first trailing edge of the U-shaped cavity impinges on the top wall. As confirmed by Mesalhy et al. [3], this eddy creates an insulation effect on the heat transfer from the second floor of the U-shaped cavity.

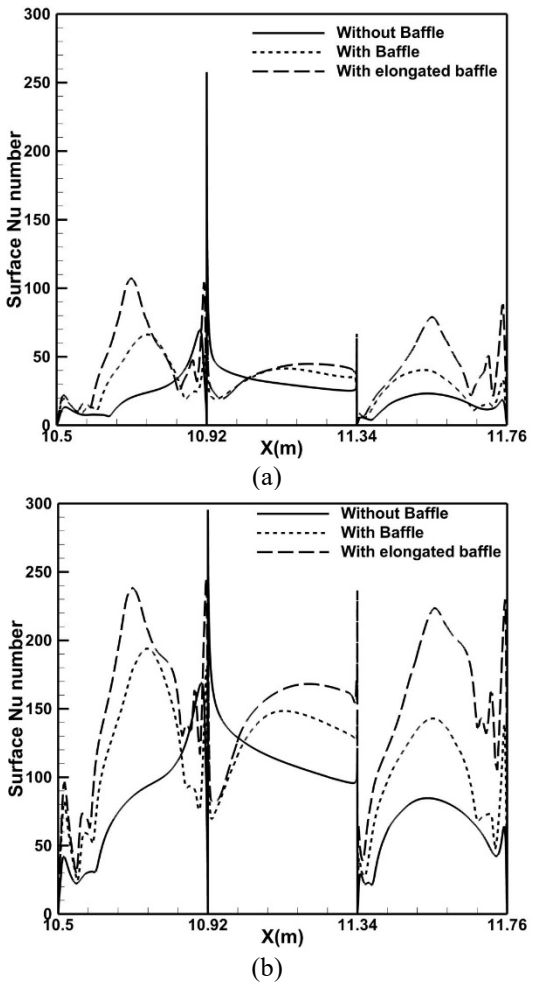


Figure 6. Effect of adiabatic baffles on the value of SNN over bottom walls for the pure mixture (without hybrid NPs) at  $U_0=0.1$  m/s (a), and  $U_0=0.6$  m/s (b).

In Figure 6, for the pure mixture, the effects of adiabatic baffles and Re number on the SNN at the cavity floors are illustrated. Consistent with Zdanski et al. [2], for low Re numbers, the heat dissipation by the convection from the cavity floor is possibly low. Increasing the Re number promotes the cooling system (mixing of hot and cold fluids) and enhances the heat dissipation.

As indicated by Zdanski et al. [42], most of the heat flux (89%) coming from the cavity floor is pumped by the turbulent diffusion. It is influential on the mechanism of the heat transfer at the cavity floor. When adiabatic baffles are installed, the impact of the externally cold binary fluid on the cavity dynamics increases significantly, and the value of SNN enhances. The distribution of the SNN shows that the peak values of the heat flux at the cavity floor are intensified due to the presence of baffles.

As can be detected, the presence of baffles considerably enhances the SNN over two floors of the U-shaped cavity. However, due to the redirected flow over the first trailing edge of the cavity, the SNN over the middle floor is initially decreased compared to the case without adiabatic baffles.

For the pure mixture, the variations of ANN with the Re number are displayed in Figure 7a. At Re=5000, adding baffles with a length equal to h=0.042m enhances the value of ANN by 47% compared to the case without baffles. At Re=30000, due to the presence of these baffles, the value of ANN augments by 35%. At Re=5000 and 30000, using elongated baffles (with a length equal to 2×h) increases the value of ANN by 87% and 67%, respectively, in contrast to the case without baffles.

As Navaneethakrishnan and Muthtamilselvan [6] discussed, using baffles with a shorter length engenders a lesser disturbance compared to elongated baffles. Hence, the mainstream channel flow is less affected, and the fluid mixing is diminished, resulting in lower heat transfer rates. When elongated baffles are introduced, the channel flow is further forced downward toward the cavity floor, and hence, the fluid mixing is boosted.

As can be seen, when the Re number increases, the presence of adiabatic baffles becomes less effective in improving the heat transfer capability of the binary fluid.

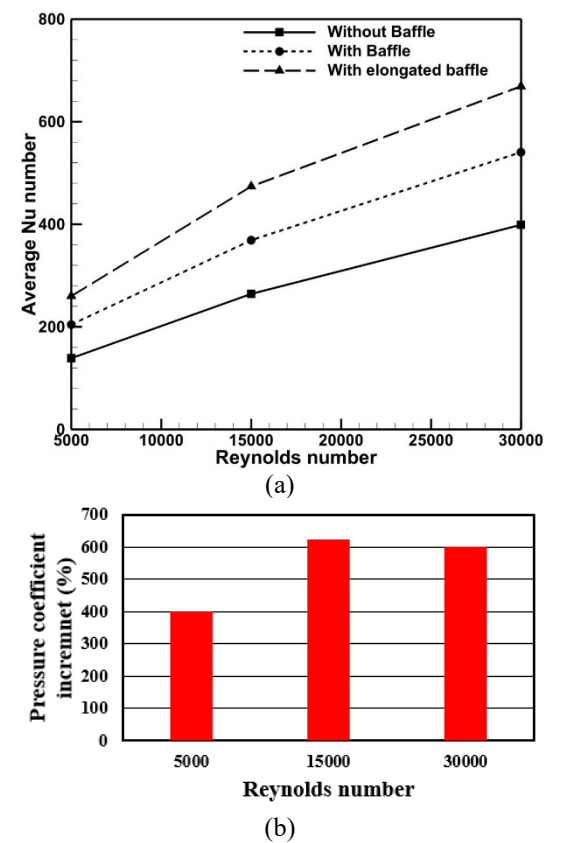


Figure 7. Variations of the ANN with the Re number for the pure binary fluid (a) and percentage of pressure coefficient increment due to the presence of elongated baffles (b).

The pressure coefficient in the horizontal channel-driven U-shaped cavity flow is defined as,

$$C_{p,hnf} = 2.0 \times (P_{inlet,ave} - P_{outlet,ave})$$

$$P_{inlet,ave} = \frac{1}{H} \times \int_{0}^{H} P_{inlet} dy \quad P_{outlet,ave}$$

$$= \frac{1}{H} \times \int_{0}^{H} P_{outlet} dy$$

$$(25)$$

Interestingly, Figure 7b corroborates that adding elongated baffles to the top wall significantly augments the pressure coefficient compared to the plain U-shaped cavity flow (without baffle) particularly at higher *Re* number.

### 5.4 Effect of NP Concentration and Mixing Ratio

The effects of the NP concentration on the value of ANN along all cavity walls are provided in Figure 8. Dispersing hybrid NPs with  $\phi$ =0.01 in the binary mixture reduces the value of ANN. The heat transfer capability of the U-shaped cavity flow is weakened.

For example, at  $U_0$ =0.6 m/s, in the absence of baffles, the value of ANN declines by 14% using  $TiO_2$ - $SiO_2$  (mixing ratio 50:50%) HyNf with  $\phi$ =0.01 compared to the pure mixture. It implies that HyNf with a mixing ratio of 50:50% is not a good heat transfer fluid, and it is contrary to the outcome reported by Nabil et al. [18]. Adding more NPs ( $\phi$ =0.03) weakens the heat transfer capability of the binary mixture insignificantly (around 5%) compared to the case with  $\phi$ =0.01.

According to Mehrez et al. [10], adding NPs to the pure mixture alters the flow behavior (reducing the flow intensity) and enlarges the thickness of TBL. More importantly, it is observed that the unfavorable effect due to dispersing NPs (reduction of ANN) intensifies as the incoming flow becomes more turbulent.

For the pure mixture and HyNf, the variations of the  $PEC_{baffle}$  with the reference velocity (velocity of the incoming flow) are included in Figure 9.

Adding smaller baffles to the top side of the cavity flow is always advantageous ( $PEC_{baffle} > 1.0$ ) at all reference velocities. However, the substitution of the plain cavity flow with the cavity equipped with elongated baffles is only recommended at lower inlet velocity (0.1).

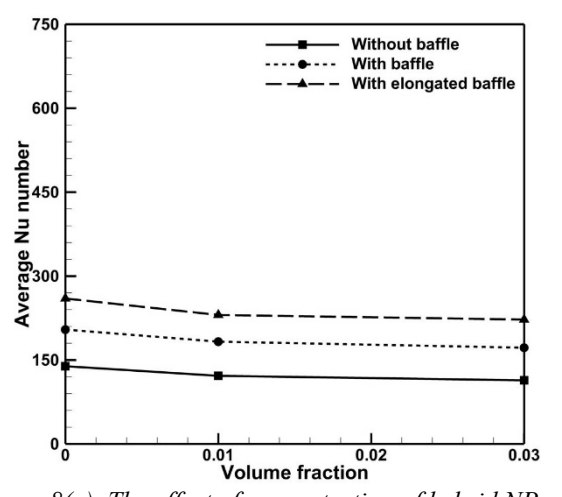


Figure 8(a). The effect of concentration of hybrid NPs on the ANN along all cavity walls at  $U_0$ =0.1 m/s.

The negative impact (pressure drop penalty) due to elongated baffles exceeds the positive effect (improved convection) at higher Re numbers. For the cavity flow with/without baffles, the effects of hybrid NPs on the thermo-hydrodynamic performance (represented by  $PEC_{nf}$ ) of the system are shown in Figure 10. It is realized that for  $0.01 \le \phi \le 0.03$ , the addition of hybrid TiO<sub>2</sub>-SiO<sub>2</sub> NPs with the mixing ratio 50:50% is not beneficial.

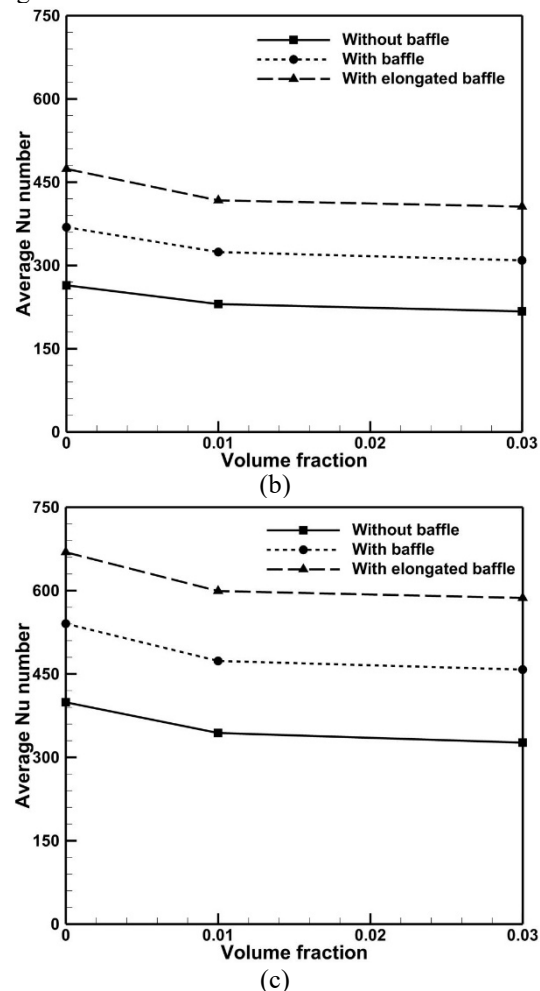


Figure 8. The effect of concentration of hybrid NPs on the ANN along all cavity walls at  $U_0$ =0.3 m/s (b), and  $U_0$ =0.6 m/s (c).

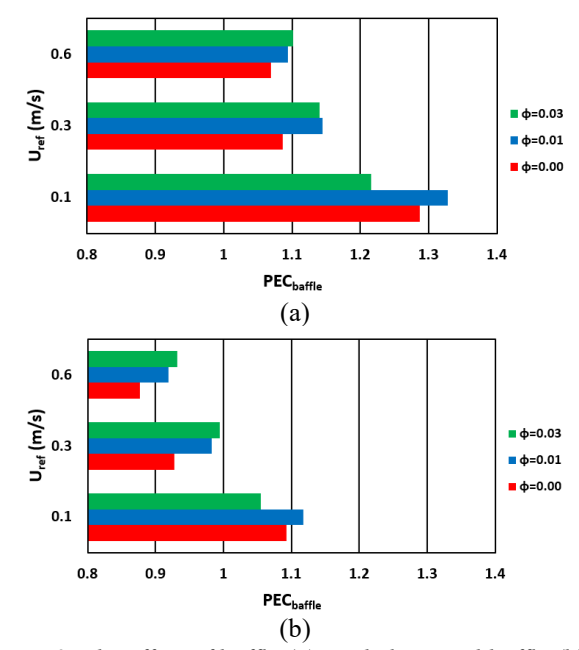


Figure 9. The effect of baffle (a), and elongated baffle (b) on the thermo-hydrodynamic performance of the cavity flow filled with pure mixture or HyNf.

Hamid et al. [20] stressed that the mixing ratio of 20:80% or 80:20% for hybrid NPs induces a PER less than 5.0, where the integrated augmentations in k and  $\mu$  has more benefits in comparison with the equal ratio (50:50%). The performances of unequal ratios, such as 20:80% or 80:20% are evaluated in Table 2 in terms of the temperature-dependent figure-of-merit (FOM).

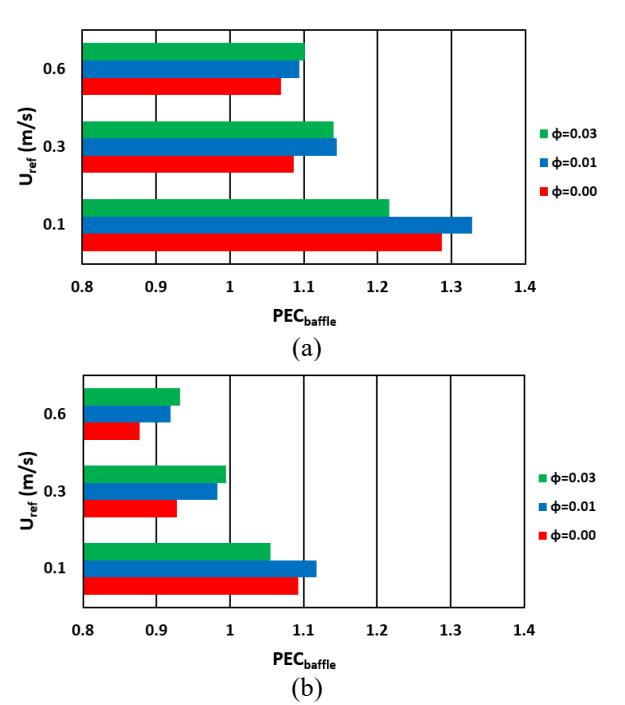


Figure 10. Replacement of the pure base fluid with HyNf at concentrations  $\phi$ =0.01 (a), and  $\phi$ =0.03 (b) in cavity flows with/without baffles.

Based on Hamid et al. [20], the mixing ratio of 20:80% gives the maximum enhancement of thermal conductivity (16%), whereas the ratio of 80:20% gives the least augmentation for the dynamic viscosity compared to other ratios.

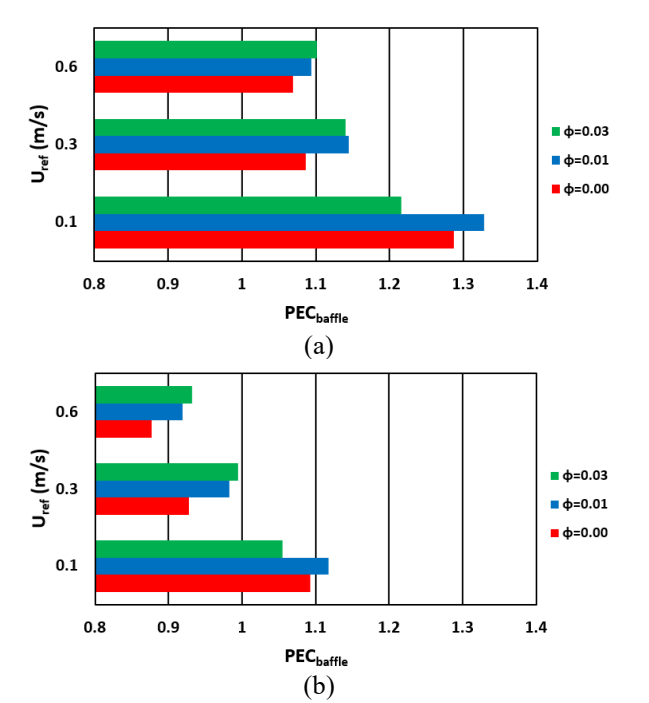


Figure 11. Variations of PEC<sub>tot</sub> at various reference velocities.

I confirm that adding TiO<sub>2</sub>-SiO<sub>2</sub> hybrid NPs (with unequal ratio) does not improve the heat transfer capability of the binary mixture. Minimizing the pressure drop through the trade-off between the shortcomings and benefits of individual NPs is not achieved here.

Table 2. Temperature-dependent variations of FOM for various mixing ratios of hybrid NPs at  $\phi$ =0.01.

Temperature (K)	TiO <sub>2</sub> -SiO <sub>2</sub> (20:80%)	TiO <sub>2</sub> -SiO <sub>2</sub> (80:20%)
303	1.00	1.006
313	0.980	0.985
323	0.995	0.986
333	0.941	0.987
343	0.915	0.954

The outcomes of this investigation recommend some strategies for the thermal design of electronic devices where two adjacent cavities with asymmetrical walls [39] exist.

#### 6. Conclusion

The heat transfer capability of the water/EG mixture in a 2D channel-driven U-shaped cavity flow, including a downward-facing cavity and an upward-facing cavity was assessed. Only the single-phase forced convection heat transfer was evaluated (the effect of natural convection within the shallow cavity was insignificant). The thermophysical properties for the aqueous solution of EG and HyNf are temperature-dependent. The available measurement data was used to acquire precise input property values in order to assess the thermal performance of HyNf. It was found that,

- (1) For the pure aqueous solution of EG, adding baffles significantly minimized the encapsulating phenomenon and enhanced the heat dissipation while it generated one recirculating eddy (as a negative outcome) over the middle floor of the cavity.
- (2) The more the velocity of the incoming flow increased, the less the presence of baffles became beneficial.
- (3) The substitution of the plain U-shaped cavity flow with the one equipped with elongated baffles was only permitted at a lower Re number.
- (4) The thermo-hydraulic performance of aqueous solution of EG was not enhanced in the presence of hybrid TiO<sub>2</sub>-SiO<sub>2</sub> NPs (with equal/unequal ratio of 50:50%) in the aforementioned asymmetrical cavity flow.
- (5) Minimizing the pressure drop through the trade-off between the shortcomings and benefits of individual NPs in the binary fluid (water/EG solution) was not achieved.

# **Conflict of Interest**

Dr. Mahmoud Jourabian approves that to the best of his knowledge, there is not any conflict of interest or common interest with an institution/organization or a person that may affect the review process of the paper.

#### **Credit Author Statement**

**Mahmoud Jourabian:** Writing - Original draft, Writing-Reviewing and Editing, Visualization, Conceptualization, Methodology, Software.

# Nomenclature

 $c_p$  Specific heat  $[J/kg \cdot K]$   $C_p$  Pressure coefficient  $[N/m^2]$  $F_1, F_2$  Blending functions

f Friction factor

- H Inlet height [m]
- h Height of middle floor [m]
- k Turbulent kinetic energy  $[m^2 \cdot s^{-2}]$
- k Thermal Conductivity  $[Wm^{-1}K^{-1}]$
- L Length of cavity floor [m]
- Mo Mouromtseff number
- Nu Nusselt number
- P Pressure  $[N/m^2]$  Pr Prandtl number
- Re Reynolds number
- $S_{ij}$  Strain rate tensor  $[s^{-1}]$
- T Temperature [K]
- u, v Streamwise and vertical velocities [m/s]
- $\bar{u}$ ,  $\bar{v}$  Time-averaged velocities [m/s]
- $U_0$  Velocity of incoming flow [m/s]
- x, y Streamwise and vertical distance [m]
- y<sup>+</sup> Nondimensional distance from the wall

# Greek symbols

- $\delta_{ij}$  Kronecker delta
- $\mu$  Dynamic viscosity [kg/ms]
- $\nu$  Kinematic viscosity  $[m^2/s]$
- $\rho$  Density  $[kg/m^3]$
- $\phi$  Volume fraction of NPs
- $\chi_1 \chi_2$  Empirical constants
- $\omega$  Specific dissipation rate [ $s^{-1}$ ]

#### Subscripts

- bf Base fluid
- nf Nanofluid
- *hnf* Hybrid nanofluid
- t Turbulent
- tot Total
- *i* Direction
- ave Average

#### Abbreviations

- ANN Average Nusselt number
- BC Boundary condition
- BFS Backward facing step
- BL Boundary layer
- CHT Convective heat transfer
- CNT Carbon nanotube
- DASC Direct absorption solar collectors
- DNS Direct numerical simulation
- EG Ethylene glycol
- FFS Forward facing step
- FOM Figure-of-merit
- HyNf Hybrid nanofluid
- LES Large eddy simulation
- MHD Magnetohydrodynamic
- MWCNT Multi-walled carbon nanotubes
- NF Nanofluid
- NP Nanoparticles
- PEC Performance evaluation criterion

#### **References:**

- [1] S. N. Sinha, A. K. Gupta, and M. M. Oberai, "Laminar separating flow over backsteps and cavities, Part ii: cavities," *AIAA Journal*, vol. 20, no. 3, pp. 370-375, Mar. 1982, doi: 10.2514/3.7918.
- [2] P. S. B. Zdanski, M. A. Ortega, and N. G. C. R. Fico, "Numerical study of the flow over shallow cavities," *Computers & Fluids*, vol. 32, no. 7, pp. 953-974, Aug. 2003, doi: 10.1016/S0045-7930(02)00067-1.

- [3] O. Mesalhy, S. S. A. Aziz, M. M. El-Sayed, "Flow and heat transfer over shallow cavities," *International Journal of Thermal Sciences*, vol. 49, no. 3, pp. 514-521, Mar. 2010, doi: 10.1016/j.ijthermalsci.2009.09.007.
- [4] C. Ozalp, A. Pinarbasi, and B. Sahin, "Experimental measurement of flow past cavities of different shapes," *Experimental Thermal and Fluid Science*, vol. 34, no. 5, pp. 505-515, July 2010, doi: 10.1016/j.expthermflusci.2009.11.003.
- [5] Y. Ma, R. Mohebbi, M. M. Rashidi, Z. Yang, and Y. Fang, "Baffle and geometry effects on nanofluid forced convection over forward- and backward-facing steps channel by means of lattice Boltzmann method," *Physica A: Statistical Mechanics and its Applications*, vol. 554, Sept. 2020, Art. no. 124696, doi: 10.1016/j.physa.2020.124696.
- [6] V. Navaneethakrishnan and M. Muthtamilselvan, "Thermal analysis of magnetohydrodynamic mixed convection in vented channel-driven cavity with corner heater: influence of adiabatic rod and flow parameters," *Journal of Thermal Analysis and Calorimetry*, vol. 149, no. 11, pp. 5755–5770, June 2024, doi: 10.1007/s10973-024-13117-4
- [7] S. Nouraei et al., "Heat transfer and entropy analysis for nanofluid flow in a semi-circular open cavity under mixed convection," Alexandria Engineering Journal, vol. 64, pp. 309–334, Feb. 2023, doi: 10.1016/j.aej.2022.09.007
- [8] S.M. Aminossadati, and B. Ghasemi, "A numerical study of mixed convection in a horizontal channel with a discrete heat source in an open cavity," *European Journal of Mechanics B/Fluids*, vol. 28, no. 4, pp. 590-598, 2009, doi: 10.1016/j.euromechflu.2009.01.001.
- [9] O. Manca, S. Nardini, K. Khanafer, and K. Vafai, "Effect of heated wall position on mixed convection in a channel with an open cavity," *Numerical Heat Transfer, Part A: Applications*, vol. 43, no. 3, pp. 259-282, 2003, doi: 10.1080/10407780307310.
- [10] Z. Mehrez, M. Bouterra, A.E. Cafsi, and A. Belghith, "Heat transfer and entropy generation analysis of nanofluids flow in an open cavity," *Computers & Fluids*, vol. 88, pp. 363-373, Dec. 2013, doi: 10.1016/j.compfluid.2013.09.026.
- [11] ASHRAE Handbook Fundamentals (SI Edition), American Society of Heating, Refrigerating and Air-Conditioning Engineers, Inc., Atlanta, 2009.
- [12] X. Xu, C. Xu, J. Liu, X. Fang, and Z. Zhang, "A direct absorption solar collector based on a water-ethylene glycol based nanofluid with anti-freeze property and excellent dispersion stability," *Renewable Energy*, vol. 133, pp. 760-769, Apr. 2019, doi: 10.1016/j.renene.2018.10.073.
- [13] S. M. Peyghambarzadeh, S. H. Hashemabadi, S.M. Hoseini, and M. S. Jamnani, "Experimental study of heat transfer enhancement using water/ethylene glycol based nanofluids as a new coolant for car radiators," *International Communications in Heat and Mass Transfer*, vol. 38, no. 9, pp. 1283-1290, Nov. 2011, doi: 10.1016/j.icheatmasstransfer.2011.07.001.

- [14] T. Yiamsawas, O. Mahian, A. S. Dalkilic, S. Kaewnai, and S. Wongwises, "Experimental studies on the viscosity of TiO<sub>2</sub> and Al<sub>2</sub>O<sub>3</sub> nanoparticles suspended in a mixture of ethylene glycol and water for high temperature applications," *Applied Energy*, vol. 111, pp. 40-45, Nov. 2013, doi: 10.1016/j.apenergy.2013.04.068.
- [15] V. Kumaresan, and R. Velraj, "Experimental investigation of the thermo-physical properties of water-ethylene glycol mixture based CNT nanofluids," *Thermochimica Acta*, vol. 545, 180-186, Oct. 2012. doi: 10.1016/j.tca.2012.07.017.
- [16] L. S. Sundar, M. K. Singh, and A. C. Sousa, "Thermal conductivity of ethylene glycol and water mixture based Fe<sub>3</sub>O<sub>4</sub> nanofluid," *International Communications in Heat and Mass Transfer*, vol. 49, pp. 17-24, Dec. 2013, doi: 10.1016/j.icheatmasstransfer.2013.08.026.
- [17] B. A. Bhanvase, M. R. Sarode, L. A. Putterwar, A. K. A., M. P. Deosarkar, and S. H. Sonawane, "Intensification of convective heat transfer in water/ethylene glycol-based nanofluids containing TiO<sub>2</sub> nanoparticles," *Chemical Engineering and Processing: Process Intensification*, vol. 82, pp. 123-131, Aug. 2014, doi: 10.1016/j.cep.2014.06.009.
- [18] M. F. Nabil, W. H. Azmi, K. A. Hamid, R. Mamat, and F. Y. Hagos, "An experimental study on the thermal conductivity and dynamic viscosity of TiO<sub>2</sub>-SiO<sub>2</sub> nanofluids in water: ethylene glycol mixture," *International Communications in Heat and Mass Transfer*, vol. 86, pp. 181-189, Aug. 2017, doi: 10.1016/j.icheatmasstransfer.2017.05.024.
- [19] M. Michael, A. Zagabathuni, S. Ghosh, and S. K. Pabi, "Thermo-physical properties of pure ethylene glycol and water—ethylene glycol mixture-based boron nitride nanofluids: an experimental investigation," *Journal of Thermal Analysis and Calorimetry*, vol. 137, no. 2, pp. 369-380, 2019, doi: 10.1007/s10973-018-7965-5.
- [20] K. A. Hamid, W. H. Azmi, M. F. Nabil, R. Mamat, and K. V. Sharma, "Experimental investigation of thermal conductivity and dynamic viscosity on nanoparticle mixture ratios of TiO<sub>2</sub>-SiO<sub>2</sub> nanofluids," *International Journal of Heat and Mass Transfer*, vol. 116, pp. 1143-1152, Jan. 2018, doi: 10.1016/j.ijheatmasstransfer.2017.09.087.
- [21] S. S. S. Sen, R. Mahato, S. Shaw, and M. Das, "Simulation of entropy and heat and mass transfer in Water-EG based hybrid nanoliquid flow with MHD and nonlinear radiation," *Numerical Heat Transfer, Part A: Applications*, vol. 85, no. 19, pp. 3253–3267, Oct. 2024, doi: 10.1080/10407782.2023.2233736.
- [22] W. H. Azmi, K. A. Hamid, N. A. Usri, R. Mamat, and K. V. Sharma, "Heat transfer augmentation of ethylene glycol: water nanofluids and applications A review," *International Communications in Heat and Mass Transfer*, vol. 75, pp. 13–23, July 2016, doi: 10.1016/j.icheatmasstransfer.2016.03.018.
- [23] R. Shi, J. Lin, and H. Yang, "Particle Distribution and Heat Transfer of SiO2/Water Nanofluid in the Turbulent Tube Flow," *Nanomaterials*, vol. 12, no. 16, p. 2803, Aug. 2022, doi: 10.3390/nano12162803.

- [24] M. Torabi, M. Torabi, M. E. Yazdi, and G. P. Peterson, "Fluid flow, heat transfer and entropy generation analyses of turbulent forced convection through isotropic porous media using RANS models," *International Journal of Heat and Mass Transfer*, vol. 132, pp. 443–461, Apr. 2019, doi: 10.1016/j.ijheatmasstransfer.2018.12.020.
- [25] F. Iachachene, Z. Haddad, M. Arıcı, M. Jamei, and A. Mataoui, "Turbulent forced convective flow in a conical diffuser: Hybrid and single nanofluids," *Engineering Analysis with Boundary Elements*, vol. 148, pp. 205–219, Mar. 2023, doi: 10.1016/j.enganabound.2022.12.027.
- [26] N. Al-Zurfi, A. Alhusseny, and A. Nasser, "Effect of rotation on forced convection in wavy wall channels," *International Journal of Heat and Mass Transfer*, vol. 149, Mar. 2020, Art. no. 119177, doi: 10.1016/j.ijheatmasstransfer.2019.119177.
- [27] Md. S. Shuvo, T. H. Ruvo, and S. Saha, "Characteristics of turbulent forced convective nanofluid flow and heat transfer in a 2D axisymmetric corrugated pipe," *Thermal Science and Engineering Progress*, vol. 41, June 2023, Art. no. 101838, doi: 10.1016/j.tsep.2023.101838.
- [28] F.R. Menter, "Two-equation eddy-viscosity turbulence models for engineering applications," *AIAA Journal*, vol. 32, no. 8, pp. 1598-1605, Aug. 1994, doi: 10.2514/3.12149.
- [29] A. Hellsten, "Some improvements in Menter's k-omega SST turbulence model," in 29th AIAA, Fluid Dynamics Conference, Albuquerque, NM, U.S.A.: American Institute of Aeronautics and Astronautics, June 1998. doi: 10.2514/6.1998-2554
- [30] P. Pires Araujo and A. L. Tenório Rezende, "Comparison of Turbulence Models in the Flow over a Backward Facing Step," *IJOER*, vol. 3, no. 11, pp. 88–93, Nov. 2017, doi: 10.25125/engineering-journal-IJOER-NOV-2017-19.
- [31] G. Sekrani, S. Poncet, and P. Proulx, "Modeling of convective turbulent heat transfer of water-based Al 2 O 3 nanofluids in an uniformly heated pipe," *Chemical Engineering Science*, vol. 176, pp. 205–219, Feb. 2018, doi: 10.1016/j.ces.2017.10.044.
- [32] D. G. Jehad, G. A. Hashim, A. K. Zarzoor, and C. S. Nor Azwadi, "Numerical study of turbulent flow over backward-facing step with different turbulence models," *Journal of Advanced Research Design*, vol. 4, no. 1, pp. 20-27, 2015.
- [33] J. Kim, S.J. Kline, and J.P. Johnston, "Investigation of a reattaching turbulent shear layer: flow over a backward-facing step," *Journal of Fluids Engineering*, vol. 102, no. 3, pp. 302-308, Sep. 1980, doi: 10.1115/1.3240686.
- [34] "OpenFOAM | Free CFD Software | The OpenFOAM Foundation." Accessed: Nov. 17, 2025. [Online]. Available: https://openfoam.org/
- [35] E. YousefiMiab, S. Baheri Islami, and R. Gharraei, "Feasibility assessment of using nanofluids in shell and tube heat exchanger of gas pressure reducing stations

- through a new developed OpenFOAM solver," *International Journal of Heat and Fluid Flow*, vol. 96, Aug. 2022, Art. no. 108985, doi: 10.1016/j.ijheatfluidflow.2022.108985.
- [36] A. Safari, M. Saffar-Avval, and E. Amani, "Numerical investigation of turbulent forced convection flow of nano fluid in curved and helical pipe using four-equation model," *Powder Technology*, vol. 328, pp. 47-53, Apr. 2018, doi: 10.1016/j.powtec.2018.01.025.
- [37] K. Akselvoll, and P. Moin, "Large-eddy simulation of turbulent confined coannular jets," *Journal of Fluid Mechanics*, vol. 315, pp. 387-411, May 1996, doi: 10.1017/S0022112096002479.
- [38] M. Jourabian, and M. Raeesi, "Turbulent forced convection flow of water-based nanofluids with temperature-dependent properties over backward-facing step channel with upwardly deflected downstream wall," *Numerical Heat Transfer, Part A: Applications*, vol. 86, no. 7, pp. 2125-2154, Apr. 2025, doi: 10.1080/10407782.2023.2287541.
- [39] W. A. Xie, and G. N. Xi, "Geometry effect on flow fluctuation and heat transfer in unsteady forced convection over backward and forward facing steps," *Energy*, vol. 132, pp. 49-56, Aug. 2017, doi: 10.1016/j.energy.2017.05.072.
- [40] C. Abdellahoum, A. Mataoui, and H. F. Oztop, "Turbulent forced convection of nanofluid over a heated shallow cavity in a duct," *Powder Technology*, vol. 277, pp. 126-134, June 2015, doi: 10.1016/j.powtec.2015.02.048.
- [41] C. Abdellahoum, and A. Mataoui, "Numerical analysis of turbulent forced convection of nanofluid flow over a heated shallow cavity," *Heat Transfer Asian Research*, vol. 45, no. 5, pp. 434-450, July 2016, doi: 10.1002/htj.21170.
- [42] P. S. B. Zdanski, M. A. Ortega, and N. G. C. R. Fico, "Heat transfer studies in the flow over shallow cavities," *Journal of Heat Transfer*, vol. 127, no.7, pp. 699-712, July 2005, doi: 10.1115/1.1924630.
- [43] D. Cornu, L. Keirsbulck, F. Kerhervé, F. Aloui, M. Lippert, "On the vortex dynamics of shear-driven deep cavity flows with asymmetrical walls," *Canadian Journal of Physics*, vol. 94, no. 12, pp. 1344-1352, Dec. 2016, doi:10.1139/cjp-2016-0305.